



A chemical approach to understanding oxide surfaces

James A. Enterkin^{a,b,c}, Andres E. Becerra-Toledo^d, Kenneth R. Poeppelmeier^{a,b,c}, Laurence D. Marks^{c,d,*}

^a Chemical Sciences and Engineering Division, Argonne National Laboratory, 9700 South Cass Avenue, Argonne, 60439, IL, United States

^b Department of Chemistry, Northwestern University, 2145 Sheridan Road, Evanston, 60208, IL, United States

^c Institute for Catalysis in Energy Processes and Center for Catalysis and Surface Science, Northwestern University, 2137 Sheridan Road, Evanston, 60208, IL, United States

^d Department of Materials Science and Engineering, Northwestern University, 2220 Campus Drive, Evanston, 60208, IL, United States

ARTICLE INFO

Article history:

Received 5 July 2011

Accepted 21 October 2011

Available online 28 October 2011

Keywords:

Bond valence sum

Coordination

Chemical bond

Surface structure

Metal oxide

ABSTRACT

Chemical bonding has often been ignored in favor of physics based energetic considerations in attempts to understand the structure, stability, and reactivity of oxide surfaces. Herein, we analyze the chemical bonding in published structures of the SrTiO₃, MgO, and NiO surfaces using bond valence sum (BVS) analysis. These simple chemical bonding theories compare favorably with far more complex quantum mechanical calculations in assessing surface structure stability. Further, the coordination and bonding of surface structures explains the observed stability in a readily comprehensible manner. Finally, we demonstrate how simple chemical bonding models accurately predict the adsorption of foreign species onto surfaces, and how such models can be used to predict changes in surface structures.

© 2011 Elsevier B.V. All rights reserved.

1. Introduction

A long outstanding challenge has been understanding in a general fashion, ideally with predictive power, the structure of solid surfaces. Oxide surfaces in particular have proven difficult to understand, often viewed as inherently different from the bulk. Theories about the driving forces behind surface structure formation include the minimization of “dangling bonds” [1] or reduction of Coulomb forces [2]. Many believe that polar surfaces must be different from the bulk since they require “charge compensation” (see for instance [3–5] and references therein). Recent results reveal that surface structures share more in common with the bulk than previously believed [6].

Two fundamental approaches exist for understanding bulk structures: physical and chemical. The former generally consists of minimizing the potential energy of a structure, and the latter of understanding the localized chemical bonds. In bulk structures, these methods are complimentary, not opposed. The physical theories are often more rigorous, but in their rigor may obscure critical insights that are readily apparent in a chemical bonding model. Each, therefore, provides useful and important information necessary for a more complete understanding of bulk structures.

The physics approach has dominated attempts to understand surface structures, with little attention paid to a chemical bonding approach. Solid state inorganic chemistry considerations may prove a great companion to the physics based investigations, potentially

leading to predictions of what surface structures may form and what reactions may occur, just as one can often predict what will form in bulk reactions.

The bond valence sum (BVS) model is commonly used to analyze coordination and bonding in solid state chemistry [7–9]. It stems from Pauling's second crystal rule [10] and it provides a good understanding of structural chemistry and chemical bonding. A bond valence is assigned to each bond, dependent only on the ions involved and the bond distance. Shorter bonds have higher valence, with the bond valence being relative to the typical bond length between the two ionic species involved. The bond valence for each bond is calculated as:

$$BV = \exp((R_0 - R)/b) \quad (1)$$

where R is the bond distance, R_0 is a standard bond distance for the types of ions involved, and b is an empirically derived constant, normally a universal constant of 0.37. R_0 values are empirically derived from structural analysis of multiple known materials. The BVS for an ion is equal to the sum of the bond valences for all the bonds surrounding the ion, with positive values for cations and negative values for anions:

$$|BVS| = \sum_{\text{all bonds}} BV \quad (2)$$

Lower values indicate reduced species and higher values indicate more oxidized species, while lower absolute values indicate lower coordination and higher absolute values indicate higher coordination.

One very important clarification needs to be made, as there is currently substantial confusion in the literature. Valence is a measure of electrons and bonds surrounding an atom and should not be confused with the charge on an atom, as the two are very different.

* Corresponding author at: Institute for Catalysis in Energy Processes and Center for Catalysis and Surface Science, Northwestern University, 2137 Sheridan Road, Evanston, 60208, IL, United States. Tel.: +1 847 491 3996; fax: +1 847 491 7820.

E-mail address: l-marks@northwestern.edu (L.D. Marks).

For instance, SrTiO₃ would be written in terms of the valence as Sr²⁺Ti⁴⁺O₃²⁻ whereas in terms of the charges on the atoms it is closer to Sr^{+1.6}Ti^{+2.2}O₃^{1.2-} if the charges are evaluated by Bader's method [11]. Valence is, in fact, what is measured by most spectroscopies, such as XPS and XANES. Charge should be reserved to describe a true electrostatic potential contribution. Charge and valence are only the same in a completely ionic model which is inappropriate for oxides. (Pauling used the term “charge” in his original papers, but it has been replaced by valence in current usage.) For polar oxide surfaces and interfaces the real issue is to find the appropriate valence neutral surface which is neither oxidized (ions substantially higher than their normal valence, e.g. Mg³⁺, O¹⁻) nor reduced (ions too low a valence, e.g. Mg¹⁺, O³⁻).

The distinction between valence and charge is easily seen in organic chemistry. In organic molecules, carbon is tetravalent, nitrogen trivalent, oxygen and sulfur divalent, and halogens and hydrogen monovalent. While the BVS formulation is not used, the same principles account for valence and bonding: triple bonds are shorter than double bonds, which are shorter than conjugated double bonds, which are shorter than single bonds. While organic carbon is tetravalent, it is not highly charged, and certainly neither +4 nor -4.

Continuing the introduction, a useful metric in BVS based structural analysis is the global instability index (GII), the root mean square of the deviation of the BVSs from the expected values for all atoms in the unit cell:

$$GII = \frac{\sqrt{\sum_1^N (BVS - BVS_0)^2}}{N} \quad (3)$$

where N is the number of atoms in the unit cell and BVS₀ is the expected BVS. In general, a lower GII is preferred, with room temperature bulk structures typically having GII < 0.2 [12,8].

Structural validation is the most common use for BVSs, and there are literally thousands of examples in the literature. Examples of other uses include the analysis of incommensurate structures, [13–15] electronegativities, [16] ligand field strengths, [17] nonlinear optical properties, [18,19] and thermoluminescence; [20,21] determination of whether NiAl₂O₄ was a normal or inverse spinel, [22] and interpretation of multiple experimental methods, including NMR [23] and XAFS [24]. More relevant to our later analysis it has been used for solid–liquid and other interfaces [25–30]. Additional information can be found in several reviews [7,12,8,9].

Despite these demonstrated uses in bulk structures, we are aware of only two times when bond valence has been applied to surface structures. The first was in Ruberto and coworkers' examination of the κ-Al₂O₃ (001)/(00-1) surfaces, [31,32] who confuse BVS with charge and consider only the bulk BVS in a discussion of polarity compensation. As neither the BVS of individual atoms nor the atomic coordinates are published, it will not be discussed further. The second is our analysis of a homologous series of structures on the SrTiO₃ (110) surface [6].

In this work, we first review the bond valence method and show how such sums can work in a complementary manner with DFT surface calculations, similar to how they are known to complement bulk DFT calculations. We then review several known and proposed surface structures on the perovskite strontium titanate (SrTiO₃) and the rock salts magnesium oxide (MgO) and nickel oxide (NiO), from a bond valence perspective. (In many cases structures are published in the literature without making the full structure and atomic positions publically available, preventing a full bond valence. Lacking the resources to repeat each experiment or calculation, we are only able to analyze those few structures which have been made publically available [33,6] or to which we have access [34–36].) Finally, we will examine a few cases where, similar to solid–liquid interfaces, adsorbates from the atmosphere may be interacting with oxide surfaces.

For simplicity, this work focuses solely on structures where each surface atom is in its optimal oxidation state. BVS is well equipped to deal with oxidation and reduction, and such analyses can be done in the future on a case-by-case basis as we believe the method will be equally useful for many other surfaces. BVS has been especially useful in bulk structures where an element occurs in multiple oxidation states within the same structure, as it provides an excellent way (sometimes the only way) to assign oxidation state to each occurrence of the element [9]. In many cases values for R₀ are available in the literature which do quite well for a range of different valence states, e.g. for Ti an R₀ value of 1.79 has been used adequately for Ti in coordination complexes with valences ranging from 2+ to 4+ [37]. More commonly, one will calculate the BVS of an atom using the R₀ for each possible oxidation state of that element, and the BVS calculated using the R₀ for the correct oxidation state is usually significantly closer to the expected whole number value than calculations using R₀ values for other oxidation states. If no R₀ gives a BVS close to the expected whole number value, this often indicates a mixed valence compound. Although this use of BVS should also be extendable to surfaces, it would add another level of complexity to this paper and will therefore be saved for a future work.

2. Methods

BVSs were calculated using the KDist program in the Kalvados program suite [38]. For structures from DFT calculations with lattice parameters different from the experimental values, the volume was changed isotropically to obtain the correct lattice parameter. Bonding interactions up to 3.5 Å were included in the calculation. A value of b = 0.37 was used in all cases. R₀ values of 1.693 Å for Mg²⁺-O²⁻, 1.654 Å for Ni²⁺-O²⁻, 2.118 Å for Sr²⁺-O²⁻, and 1.815 Å for Ti⁴⁺-O²⁻, [7] were used.

Hydrogen bonding creates a slight difficulty, requiring different parameters for R₀ and perhaps even b for hydrogen bonds of different lengths due to the asymmetry of X-H···X bonds, which is best modeled by different values for the short and long portions of the hydrogen bond (see Brown [9] Section 21 for more details). It is unclear which of the various literature values for R₀ is best. For this work, we use R₀ = 0.957 Å, the length of a O-H bond in gaseous H₂O. We chose this as gas phase H₂O, similar to the surfaces being considered, has no significant H···X interactions. For ease of calculation, b = 0.37 was maintained. While determining a R₀ value from a single parameter is far from an optimal solution, it is sufficient for the small number of hydroxylated surface structures considered here.

The GII and surface instability index (SII) were calculated by hand from the BVSs and the atomic multiplicities; the SII is calculated similar to the GII, except that only the atoms in the outermost surface and the first bulk layer are included. The top bulk layer is included in order to capture the instability associated with the strain imposed upon the bulk by the surface. Since strain decays exponentially from the surface (Saint-Venant's principle; strictly speaking an analytical solution can be written exploiting the form given for spherical harmonics by Love Section 172 [39] as a sum of the two biharmonics z·exp(-g|z + ig·ρ) and exp(-g|z + ig·ρ) with z normal to the surface [40] and g an in-plane reciprocal lattice vector), using the top two layers (surface plus top bulk layer) should provide the most information about the stability. (With very large unit cells where |g| may be small one might need more than two layers.) This was confirmed empirically: instability indices for the surface only, and for the top three layers were calculated for each structure. Neither was found to be as representative of the surface stability as the SII using the top two layers. For completeness, there is other evidence that near the surface bond lengths can converge relatively fast, [41] consistent with our use of just the outermost two layers. A bulk instability index (BII) was also calculated for the central most stoichiometric unit in the model. In all cases the expected whole number values

were used for BVS₀ and N represents the total number of atoms included in the instability index calculation.

For the SrTiO₃ (100) surface structures, DFT structural relaxations were performed using the all-electron Wien2k [42] code with an augmented plane wave basis set and were based upon a general gradient approximation (GGA) defined by the PBE functional [43]. For the SrTiO₃ (110) TiO faceted model with too few layers and SrTiO₃ (111) model 8 with more layers, an on-site PBE0 functional with exact-exchange TPSSH hybrid for final energy calculation was used, to maintain consistency with the calculations from the original publications [33,6]. All other structures analyzed were the previously published structures, and calculation parameters may be found in the original publications.

CIFs are available for all structures analyzed herein; for further details see Supplemental Information.

3. The bond valence sum method and DFT structural relaxations

The bond valence model provides complementary information to density functional theory calculations for bulk structures. For instance, it has been used to correct DFT bond lengths, [27] and GII follows the same trends DFT calculated energy for bulk structural instabilities [44].

The bond valence model also works well for surface analysis, as indicated by the complementary nature of BVSs and DFT structural convergence. Fig. 1 shows data during a DFT structural minimization of a hydroxylated MgO (111) surface structure [45]. The GII and DFT calculated energy have nearly identical trends, demonstrating that most of the energy reduction can be attributed to optimization of local bonding. The improved bonding occurs primarily at the surface, as indicated by the SII. The bulk instability index increases as expected; long-range strains from the surface rearrangements perturb the bonding in the center of the slab.

A technical digression. A standard method with ab-initio calculations is to look at the surface stress of different configurations/parts of the structure, for instance that of the surface monolayer. This method stems in large part from an epitaxial approach. This is easy since most pseudopotential codes give the stress for free. One can then compare energetics with a nominal expansion/contraction and show how the surface stress can be used to explain transitions. The surface stress is a derivative (in the appropriate units, see [46]) of the energy with respect to strain, which can be decomposed into a chain-rule sum of derivatives of individual bond-lengths in a local bond-valence method. Hence an overcontracted or overexpanded surface will show a large surface stress contribution to the energy, and non-ideal BVS values at a surface. Even for the lowest energy configuration the outermost atomic layer can implicitly apply tractions to the

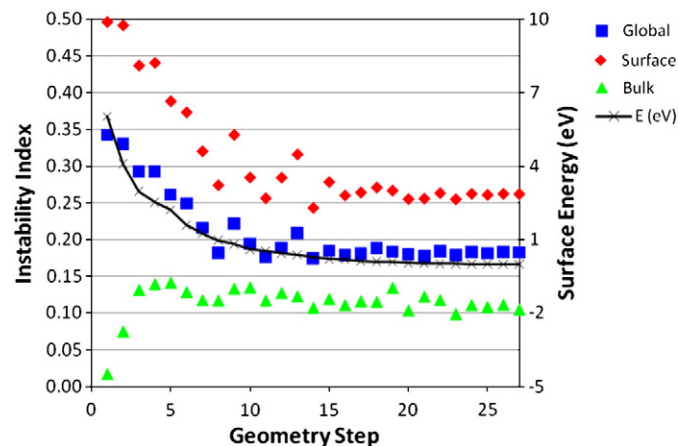


Fig. 1. Global, surface, and bulk instability indices and energy plotted as a function of geometry optimization step for a hydroxylated MgO (111) surface from [45]. Energy is relative to the final energy.

layers below. In a classical formulation this would lead to oscillatory relaxations biharmonically decaying into the bulk as mentioned above; in a BVS formulation it shows up as a deviation of the BII from its optimum value as seen in Fig. 1.

BVSs can also determine if sufficient layers have been used in the DFT surface calculations. If so, then the center of the slab will have BVSs the same as the bulk structure; otherwise the BVSs will differ from those of the bulk structure.

As an example, a model of the SrTiO₃ (110) TiO faceted structure was originally optimized with only three bulk SrTiO⁴⁺ and four bulk O₂²⁻ layers, before expanding the calculations to five bulk SrTiO⁴⁺ and six bulk O₂²⁻ [6]. In the former case, the number of layers was too few as shown from a BVS analysis (Fig. 2). To further the comparison, a case with only one bulk SrTiO⁴⁺ and two O₂²⁻ was calculated as well. While the BVSs of the surface species were improved for models with smaller numbers of layers, the bulk coordination was far from the bulk BVSs. A necessary, but not sufficient, condition for an accurate model is that the atoms at the central layer have BVSs similar to the bulk.

Additionally, we have found that performing a structural optimization by minimizing the GII prior to performing a DFT structural relaxation can significantly decrease the cost of the DFT calculation. This can be done by hand, changing the position of a few atoms in an initial structural model so they have reasonable BVS values. In principle a BVS based structural optimization could be carried out in a matter of seconds on a standard laptop computer even for large structures, although at present we are not aware of a code for this. Such a program may also provide a particularly useful alternative to force-field type calculations of surfaces and defects, as good force-fields for surfaces and defects are often lacking.

Finally, BVS may provide a check on the accuracy of a DFT functional. Because current DFT methods have problems in accurately calculating solid materials in general and solid surfaces in particular, much work has been undertaken to develop more accurate functional for solids and solid surfaces [47–49]. Since BVS parameters are empirically derived from crystal structures and are universal, they should provide a good check on these new functionals. A more accurate functional should give BVS values for bulk structures that are closer to those derived from crystal structures. Similarly, such a functional would be expected to give a lower SII for surface structures experimentally known to be stable, at least as compared to those which are known from experiment to be unstable.

4. Bond valence sums of model oxide surfaces

We now turn to specific surface examples, discussing the SrTiO₃ (110), (111), and (100); MgO (111); and NiO (111) surfaces.

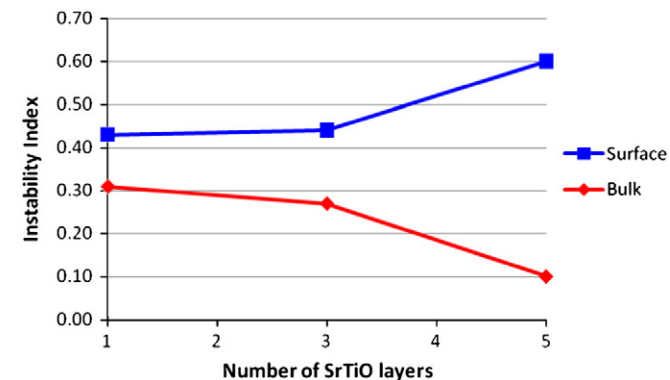


Fig. 2. Change in SII and BII with number of layers in calculation slab for the SrTiO₃ (110) halfO₂ surface.

4.1. SrTiO₃ (110)

The only other published example of BVs of a surface is for the STO (110) surface [6]. There, a homologous series of (n × 1) structures was compared to a few other proposed surface structures, and the experimentally observed structures had both the lowest DFT calculated energy and BVs closest to the expected whole number values. Using this as a starting point, we re-calculate the BVs of the (n × 1) homologous series, and some that were considered for comparison. The structures here analyzed include the (n × 1) series (n = 2, 3, 4, 5, 6, ∞), two structure types terminated by a half-filled O₂ layer, and two Sr-terminated models.

The structure of the homologous series consists of chains of corner sharing TiO₄ tetrahedra, which are interspersed by rings of similar corner sharing TiO₄ tetrahedra after every n chain tetrahedra. Half-O₂ type A is terminated in a bulk-like O₂ layer, but with half of the O removed. Two versions of this were considered, with the O removed in straight lines [50–58] or in zig-zags forming a (2 × 1) unit [56,6]. Heifets et. al. [50–52,55,56] also considered another type of half-O₂ termination (type B), which has a single O per unit cell, but bridging between two Sr atoms instead of in a bulk-like position. The Sr facet model is a Sr-adatom in a bulk-like position [50–58]. Bottin et. al. [57] proposed more deeply faceted models similar to the first Sr model forming (1 × n) supercells, the first two members of which are considered here.

BVs of the homologous series of n × 1 structures were discussed in [6], here we have used a slightly larger cut-off distance, and therefore get slightly different values (Table 1). The n = 3 and n = 4 structures have the best BVs, while the BVs gradually get worse as n increases or decreases. The BVs absolute values decrease as n increases (Fig. 3). This is not surprising, as the excess TiO₂ at the surface also decreases with increasing n: the lower the value of n, the more Ti and O atoms are packed into the same area. The O at the middle of the ring has, in all cases, the highest coordination of the surface O. Its BVs drops close to expected levels as n increases above 3, and the BVs of other atoms which are part of the ring remain close to expected values, but at the same time the BVs of those atoms which are not part of the ring drop below the expected values. In the end limit of the series (n = ∞) the BVs of the Ti drops to 3.19 and that of O to –1.21, closer to Ti³⁺ and O¹⁻ than to Ti⁴⁺ and O²⁻. Additionally, the O directly below the ring center becomes increasingly under-coordinated as n increases. At the other end of the series, n = 2, the structure becomes over-coordinated. Most notably, the O in the middle of the ring is very over-coordinated (BVS = –2.39), as is the O in the middle of the chain (which for n = 2 has shrunk to a ring as well,

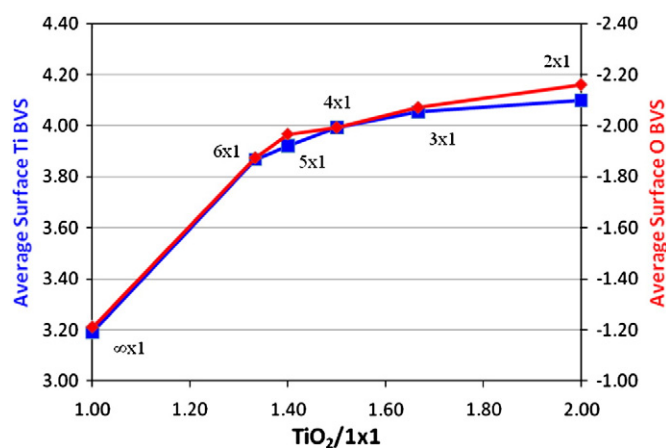


Fig. 3. Changes in coordination of surface species in (n × 1) series as a function of excess TiO₂.

BVS = –2.21). This leads to a higher SII for the n = 2 structure than for the n = 3, 4 or 5 structures.

The structure composed only of rings is over-coordinated, and might be difficult to form. This fits with the DFT energy calculations where, even though it is on the convex hull by default as the most TiO₂ rich structure calculated, the 2 × 1 structure is significantly higher in energy than the other members of the homologous series [6]. Conversely, structures with mostly straight TiO chains are under-coordinated, and therefore unstable. The optimum BVs are reached when the TiO chains are broken up by rings at regular intervals. This again agrees with the DFT energy calculations (Fig. 4), where the (3 × 1) and (4 × 1) structures, which have the overall best coordination and surface instability indices, lie on the convex hull, but higher n structures are above the convex hull. The (5 × 1) and (6 × 1) structures are only slightly above the convex hull (within calculation error), but the energy and surface instability indices are on steep upward trends and the (∞ × 1) structure is above the convex hull by more than 1 eV.

These findings bear many similarities to the TiO₂ anatase (001) reconstructions analyzed by Lazzeri and Selloni [59]. They describe a homologous series of surface structures of (1 × n) structures (n = 3, 4, 5, 6, ∞) (although they do not term it such) which differ in how frequently a row of TiO₂ units is added to the bulk termination (the (1 × 1) being the n = ∞ case). While they do not mention BVs, they report that the bond lengths increased as n increased, which

Table 1
BVVs and multiplicity of SrTiO₃ (110) (n × 1) structures.

SII	2 × 1			3 × 1			4 × 1			5 × 1			6 × 1			∞ × 1		
	0.13			0.07			0.07			0.10			0.17			0.57		
	Atom	Mult	BVS															
Surface	Ti1	2	4.08	Ti1	2	4.08	Ti1	2	4.07	Ti1	2	4.04	Ti1	2	4.03	Ti1	1	3.19
				Ti2	2	4.04	Ti2	2	3.97	Ti2	2	3.97	Ti2	2	3.96	Ti2	2	3.96
	Ti2	2	4.12	Ti3	1	4.04	Ti3	2	3.94	Ti3	2	3.85	Ti3	2	3.80	Ti3	2	3.80
				Ti4	1	3.82	Ti4	1	3.82	Ti4	1	3.82	Ti4	2	3.68			
	O1	2	–1.99	O1	2	–2.03	O1	2	–2.03	O1	1	–2.10	O1	1	–2.09	O1	1	–1.21
				O2	2	–2.02												
	O2	2	–2.05	O2	2	–2.02												
				O3	1	–2.21	O3	1	–2.19	O3	2	–1.94	O3	2	–2.03	O3	2	–2.03
O3	1	–2.21	O3	1	–2.19	O3	2	–1.94	O3	2	–2.03	O3	2	–2.03	O3	2	–2.03	
			O4	1	–2.39	O4	2	–2.04	O4	1	–2.13	O4	2	–1.93	O4	2	–1.90	
O4	1	–2.39	O4	2	–2.04	O4	1	–2.13	O4	2	–1.93	O4	2	–1.93	O4	2	–1.90	
			O5	1	–1.84	O5	1	–1.84	O5	1	–1.75	O5	2	–1.63	O5	2	–1.63	
Linking O ₂ layer	O5	2	–1.95	O5	2	–2.11	O6	2	–2.10	O6	2	–2.10	O6	2	–2.10	O6	2	–2.06
				O7	1	–1.99	O7	2	–1.95	O7	2	–1.96	O7	2	–1.95	O7	2	–1.95
	O6	2	–2.01	O6	2	–1.99	O6	2	–2.10	O6	2	–2.10	O6	2	–2.10	O6	2	–2.06
				O7	1	–2.06	O7	2	–1.95	O7	2	–1.96	O7	2	–1.95	O7	2	–1.95
	O7	1	–2.01	O7	1	–2.06	O7	2	–1.95	O7	2	–1.96	O7	2	–1.95	O7	2	–1.95
				O8	1	–2.01	O8	2	–2.04									
	O8	1	–2.01	O8	1	–2.01	O8	2	–2.04									
				O9	2	–2.11												
	O9	2	–2.07	O9	2	–2.07	O9	2	–2.11									
				O10	1	–2.02												
O10	1	–2.02	O10	1	–2.02	O10	1	–2.02	O10	1	–2.02	O10	1	–2.02	O10	1	–2.02	
			O11	2	–2.02													
O11	2	–2.02	O11	2	–2.02	O11	2	–2.02	O11	2	–2.02	O11	2	–2.02	O11	2	–2.02	
			O12	2	–2.13													

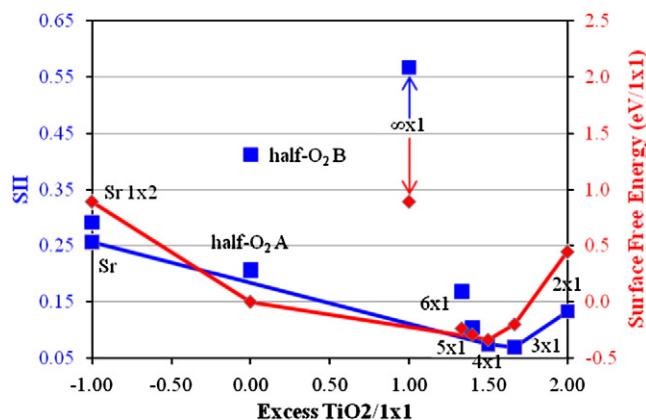


Fig. 4. Comparison of surface free energy [6] and SII for SrTiO₃ (110) surface structures with convex hull construction.

would result in decreased coordination and lower BVS. This is the same as observed for the SrTiO₃ (110) homologous series. Just as interspersing the chains with rings more often increased coordination in SrTiO₃ (110), interspersing the bulk-like termination with TiO₂ rows increased coordination on anatase (001). As mentioned earlier, the strain and surface stress referred to by Lazzeri and Selloni can be correlated to coordination and bond lengths. Positive strains ($n > 4$) indicate compressing the surface would make it more stable, while negative strains ($n = 3$) indicate that expanding the surface would improve coordination. This fits with their reported average bond lengths. While Lazzeri and Selloni conclude in their work that the number of under coordinated surface titanium atoms cannot explain the series of reconstructions, they considered only number of bonds, and not bond strength. A BVS analysis would include also bond strengths, and would likely provide as helpful in understanding this surface and other strained surfaces as in understanding the SrTiO₃ (110) homologous series.

For the stoichiometric structural models, type A is superior to type B (Table 2). For type A, the two possible arrangements of missing O atoms lead to very similar BVSs (SII = 0.21 for both), close to the expected values. This implies that a half-filled O₂ layer might be reasonable, and further that it is not highly dependent on the ordering of the missing O. A half-O₂ type A structure with disorder in the O vacancy locations might be expected for an unreconstructed cleaved sample. Half-O₂ type B, on the other hand, has BVSs that are very far from the expected values (SII = 0.41), indicating any structure similar to this must be considered highly doubtful, in agreement with Heifets and coworkers' calculations that this termination is significantly higher in energy than the half-O₂ type A [55]. These results coincide with DFT calculations where the half-O₂ type A structures lies on the convex hull (Fig. 4) [6].

For the two Sr faceted models (Table 2), the topmost Sr has a BVS close to the expected value, but the O from the top O₂ layer bonded to the surface Sr are under-coordinated, while the O on the top SrTiO bulk layer (directly below the surface Sr) are over-coordinated. The surface Sr relaxes towards the bulk to achieve sufficient coordination, while the top bulk O from the O₂ layer relaxes upward towards the surface Sr and away from the bulk, leaving it under-coordinated. The degree of this under-coordination is greater for the (1 × 2) faceted model than for the (1 × 1) model. However, for the (1 × 2) model they represent only half the number of atoms. Other atoms maintain BVSs close to the expected values. Therefore the less frequent an apex of the facet occurs, the more stable the structure will be. This, however, is not sufficient to explain why the (1 × 2) model was calculated to be more stable, [57] as the SII remains greater for the (1 × 2) model (SII = 0.29) than the (1 × 1) model (SII = 0.26). One possible explanation for this is that the simple BVS calculation does not fully reveal the instability of the Sr atom at the apex.

There are two chemical reasons why this would be unstable. First, the apical Sr atom has become unusually close to the Ti atom in the layer below it (3.00 Å Ti–Sr distance in the (1 × 1) model and 3.05 Å in the (1 × 2) model, compared to 3.38 Å in bulk SrTiO₃). There is no easy way to quantify this using BVSs, as cation–cation or anion–anion interactions are neglected.

Second, more than half of the Sr atom's coordination sphere is empty. A stable atomic coordination will have electrons filling space in all directions. This phenomena is well known, and has been considered at least since the introduction of valence shell electron pair repulsion theory [60]. For metal cations, this means bonds to O anions equally in all directions. As lone electron pairs can also fulfill this requirement for O anions, the lack of bonds in all directions should have less of an effect for O anions. For completeness, we note that this can also be considered in terms of screening; the nuclear charge of an oxygen anion with an incomplete coordination sphere can be somewhat screened by the non-bonding valence electrons, whereas a Ti/Sr cation has far fewer valence electrons available to do this. Since BVS ignores these geometric concerns, metal terminated structures will be less stable than indicated by a simple BVS analysis, and this is seen in the differences between the SII and the DFT calculated energies. Such an instability might be modeled by a vectorial bond-valence model, such as that proposed by Harvey and coworkers [61]. However, as this vectorial approach is not as easily quantified by the tools currently available to us, it will be considered only in a qualitative manner in this work.

4.2. SrTiO₃ (111)

The only proposed surface structures for SrTiO₃ (111) for which atomic coordinates are available in the literature are the 10 small structures calculated by Marks et al. [33,62] Six of these structures (models 3–8) are fully oxidized, three (models 1, 9 and 10) are

Table 2
BVSs and multiplicity of other SrTiO₃ (110) surface structures.

SII	halfO2A			halfO2A-2 × 1			halfO2B			Sr			Sr_faceted		
	0.21			0.21			0.41			0.26			0.29		
	Atom	Mult	BVS	Atom	Mult	BVS	Atom	Mult	BVS	Atom	Mult	BVS	Atom	Mult	BVS
Surface	O1	1	-1.96	O1	2	-1.94	O1	1	-1.64	Sr1	1	2.00	Sr1	2	1.88
													O1	2	-1.49
													Sr2	2	1.93
													Ti1	1	4.18
													O2	1	-2.61
													O3	2	-2.26
													O4	2	-1.77
1st bulk layer	Sr1	1	2.15	Sr1	2	2.12	Sr1	1	2.52	O1	2	-1.73			
	Ti1	1	3.81	Ti1	2	3.83	Ti1	1	3.30						
	O2	1	-1.75	O2	2	-1.82	O2	1	-1.76						

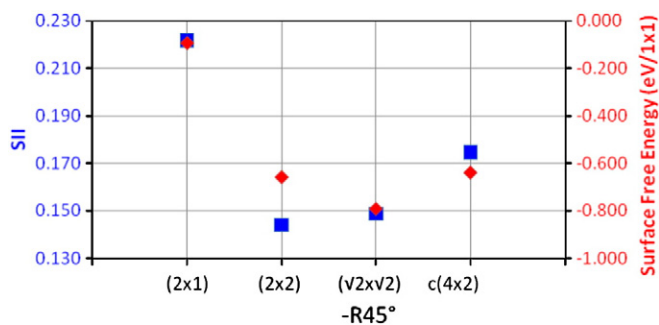


Fig. 6. Comparison of surface free energy and SII for SrTiO₃ (100) TiO₂ rich reconstructions.

calculated energy. Of the five models with similar SII, model 8 is the best coordinated. Along with model 8, model 3 would form a convex hull construction were incomplete cation coordination spheres accounted for in SII. This agrees with the DFT calculations, [33] where models 3 and 8 form the convex hull.

4.3. SrTiO₃ (100)

Of all the SrTiO₃ surface orientations, the (100) surface is the most studied, with the greatest number of surface structures. The fully oxidized structures include the crystallographically solved (2 × 1), [64,65,34,66,67,36,68] (2 × 2), [69,36,70,71,68] and c(4 × 2), [72,65,73,66,35,36] the bulk-like (1 × 1) Sr- and Ti-terminations, [74–78,67,68] and the calculated ($\sqrt{2} \times \sqrt{2}$)-R45° [36,68] structures. Reduced structures include Sr-adatoms, [79–81] O vacancies in a Ti-terminated surface, [82–86] and the c(6 × 2) structure [87]. BVS provides an excellent method for determining oxidation state, and a BVS study of the reduced structures would be most interesting, but lies beyond the scope of this work. Other surface reconstructions have been observed, but atomic positions are unknown (Fig. 6).

Of the two bulk-like (1 × 1) structures (Table 4), [74–78,67,68] the Ti-termination is distinctly more stable. The surface is somewhat under-coordinated (BVS = −1.88 for O, BVS = 3.75 for Ti) and the SrO layer below slightly over-coordinated (BVS = 2.25 for Sr, BVS = −2.37 for O), leading to a high SII of 0.24. The Sr termination is severely under-coordinated at the surface, especially for the O atom (BVS = 1.78 for Sr, BVS = −1.50 for O). The O atom in the bulk TiO₂ layer below is slightly overcoordinated (BVS = −2.22) due to the proximity of the surface Sr atom. The SII, at 0.29, is significantly higher than for the Ti-termination. While both are under-coordinated at the surface, the Sr termination is far more so, indicating that in general the Ti termination would be more stable. This

preference for the TiO₂ termination may help explain why there are more reports of surface reconstructions based on a TiO₂ termination than based on a SrO termination, although we should mention that most preparations yield TiO₂ rich surfaces which precludes the other class.

The ($\sqrt{2} \times \sqrt{2}$)-R45° surface structure [36,68] (Table 4) has never been seen experimentally observed, despite having been calculated to be the lowest in energy. It shows very good BVSs with a SII of 0.15, but has over-coordinated bulk Sr and O atoms (all Sr have BVS ≥ 2.32), which leads to a high GII (GII = 0.21). This surface structure couples to an antiferroelectric bulk distortion which persists to large depths in a DFT calculation. The Sr BVS is similar that of the DFT minimized structure of SrTiO₃ which, at least with the PBE functional, is well known to be incorrect. Specifically, the c/a ratio and degree of octahedral tilting for the ferroelectric distortions in perovskites are overestimated by GGA methods [88–90]. The discrepancy in the bulk suggests that the apparent stability of this structure may be due to problems with DFT functionals, a topic where there is currently a substantial amount of new work appearing; [91,47,49,92] we cannot say more here beyond raising these issues, which will reappear with NiO surfaces later.

The (2 × 2) structure [69,36,70,71,68] (Table 4) is fully converged to bulk-like BVSs by the second bulk TiO₂ layer. The surface shows nearly ideal BVSs, and the top bulk layers are only slightly over-coordinated (BVS = 4.29 for Ti, BVS = −2.31 for O, BVS = 2.37 for Sr), leading to a low SII of 0.14. There are some over-coordinated atoms in the second bulk layer, which lead to an increased instability index of 0.20 when this layer is included. Still, the (2 × 2) surface structure should be relatively stable.

The c(4 × 2) structure [72,65,73,66,35,36] (Table 4) is also quite reasonable (SII = 0.17). The surface layer has good BVSs, except for the O atom in the middle of all four TiO₅ polyhedra, which is significantly over-coordinated (BVS = −2.56). The top bulk TiO₂ layer has some over-coordinated Ti atoms (BVS = 4.35 and 4.30), but in general BVSs are close to the expected values. It converges more quickly to bulk-like BVSs than does the (2 × 2) structure, and the instability index when including the second bulk layer is 0.18. Overall, the BVSs are similar to the (2 × 2) structure, which agrees well with DFT calculations where the two structures are similar in calculated surface energy (within 0.06 eV).

The (2 × 1) structure [64,65,34,66,67,36,68] (Table 4) is surprisingly under-coordinated at the surface for a structure which has been crystallographically solved. The top two surface O atoms, including the “dangling oxygen” are both under-coordinated (both with BVS = −1.74) as is the Ti atom bonded to the “dangling oxygen” (BVS = 3.65). There is some over-coordination in the top bulk layers. The SII is 0.22, and increases to 0.24 when including the second bulk

Table 4
BVSs and multiplicity of SrTiO₃ (100) surface structures.

SII	SrO (1 × 1)			TiO ₂ (1 × 1)			(2 × 1)			(2 × 2)			($\sqrt{2} \times \sqrt{2}$)-R45°			c(4 × 2)				
	Atom	Mult.	BVS	Atom	Mult.	BVS	Atom	Mult.	BVS	Atom	Mult.	BVS	Atom	Mult.	BVS	Atom	Mult.	BVS		
0.29																				
	Sr1	1	1.78	Ti1	1	3.75	Ti1	1	3.92	Ti1	2	4.03	Ti4	2	4.00	Ti1	4	4.07		
	Sr2	1	1.78				Ti2	1	3.65	Ti2	2	3.94				Ti2	4	4.03		
	O1	1	−1.50	O4	1	−1.88	O1	1	−1.74	O1	4	−1.95	O11	2	−1.93	O1	8	−1.93		
							O2	1	−1.74	O2	2	−2.17	O2	2	−2.14	O2	2	−2.20		
							O3	1	−2.25	O3	2	−2.01	O10	2	−2.14	O3	4	−2.02		
							O4	1	−2.02	O4	1	−2.02	O4	2	−2.56	O4	2	−2.56		
										Ti3	1	4.11	Ti3	2	3.98	Ti3	2	4.35		
																Ti4	4	4.02		
																Ti5	2	4.30		
																O5	4	−2.03		
																O6	4	−2.15		
																O7	4	−2.20		
																O8	4	−1.94		
																O9	2	−2.25		
																O8	4	−1.94		

Table 5
BVSS for MgO Octapolar structure models.

SII	Mg-Oct			O-Oct			MgH-Oct			OH-Oct		
	0.13			0.16			0.16			0.09		
Layer	Atom	Mult	BVS	Atom	Mult	BVS	Atom	Mult	BVS	Atom	Mult	BVS
Surface	Mg1	1	1.83	O1	1	-1.70	Mg1	2	1.84	H2	2	1.02
										H1	2	1.02
										O14	2	-1.87
Sub-surface	O1	3	-1.96	Mg1	3	1.91	H1	2	1.04	O1	2	-2.15
							H2	2	1.00	Mg1	4	1.96
							O2	2	-2.17	Mg2	2	2.07
							O1	4	-1.82			
							O15	2	-2.43			

layer. This is in agreement with DFT calculations, which find the (2×1) structure ~0.6 eV higher in energy than the (2×2) or c (4×2). The undercoordination suggests that this structure may be unstable as is, needing to form additional bonds to increase its coordination; this is a topic for a separate paper [93].

5. Adsorbates on surface structures

A first step towards understanding the reactivity of surfaces is to understand their ability to adsorb foreign species. The limiting factor for performing a bond valence analysis of the adsorption of foreign species to a surface is often the lack accurate structures from which BVSS may be calculated. Recent studies of hydroxylated surfaces of MgO (111) [45] and NiO (111)[94] have made the necessary structural information available for several structures on these surfaces. These structures provide an excellent starting point for a chemical bonding analysis of water adsorbing and dissociating on oxide surfaces.

5.1. H₂O on MgO (111)

In the (111) direction, MgO is composed of alternating magnesium and oxygen layers. Ciston and co-workers [45] examine six possible dry MgO (111) terminations: the Mg and O terminated octapoles, a Mg terminated (2×2)-α and three O terminated (2×2)-α reconstructions. The octapolar reconstructions, first proposed by Wolf, [2] have a p(2×2) periodicity with surface atoms in bulk-like positions, but are missing 3/4 of the atoms in the top layer and 1/4 of the atoms in the second layer, essentially creating (100) nanofacets. While such structures are predicted to be stable and have been the subject of much theoretical work, they have never been definitively observed experimentally. What has instead been observed are (2×2)-α type structures, in which atoms in the terminal layer can occupy any or all of three different possible sites and the different occupations are virtually indistinguishable crystallographically.

The (2×2)-α-Mg structure has all three sites occupied by Mg atoms, is reduced, and therefore will not be considered here (and does not appear to exist). The (2×2)-α-O structures are stoichiometric, and have two sites occupied by O atoms and the third site vacant.

The two octapolar structures are calculated to be energetically favorable [95,96,45]. The BVSS (Table 5 and Fig. 7) are similarly quite good. Whereas the O terminated octapole is calculated to be slightly lower in energy via DFT, the SII of the Mg terminated octapole is slightly superior (0.13 vs. 0.16). The Mg terminated octapole has a terminal cation with most of its coordination sphere empty. As seen with strontium titanate surfaces geometry considerations indicate that such surfaces are less stable than indicated by their SII. Taking this into account, the bond valence analysis qualitatively agrees with the DFT calculations, with the O terminated octapole more stable than the Mg terminated octapole.

For the (2×2)-α-O reconstructions, two of the three possible sites are occupied to maintain stoichiometry. The three models differ only in which site is left vacant: site 1 is vacant in model 1, site 2 in model 2, and site 3 in model 3 (Table 6 and Fig. 7). The BVSS agree with the DFT energies, with the SIIs falling in the same order as the DFT energies. In models 1 and 2, the BVS for the O atom in sites 1 and 2 is significantly closer to the expected value of 2 than the O atom in site 3. It fits that model 3, where site 3 is vacant, should have the best overall SII (0.25, compared to 0.46 and 0.49 for models 1 and 2, respectively). In model 3, the under-coordination is less severe and more spread throughout the surface structure. The O atom in site 2 (BVS = -1.67) is slightly better coordinated than the O atom in site 1 (BVS = -1.51). That site 2 is better than site 1 is confirmed by comparing models 1 and 2. The overall ordering of the coordination of the three oxygen sites is site 2 > site 1 >> site 3.

Eight hydroxylated structures are also examined: The hydroxylated (1×1) structure, Mg and O terminated (√3×√3)-R30° structures, hydroxylated Mg and O terminated octapoles, and three (2×2)-α-OH structures. The (1×1)-H structure is a simple (1×1) oxygen

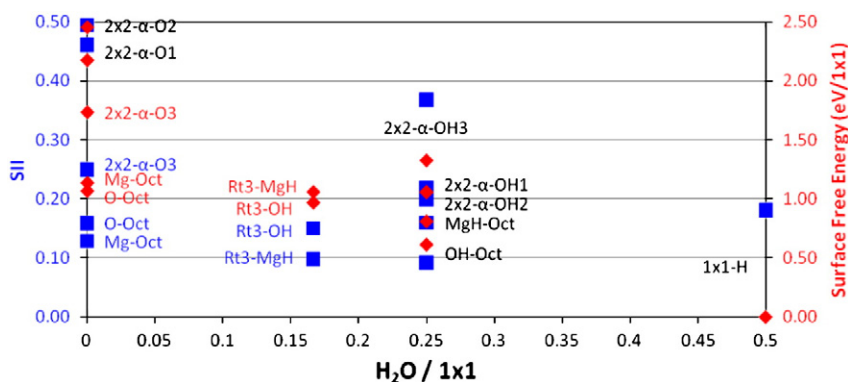


Fig. 7. Comparison of surface free energy[45] and SII for MgO (111) surface structures.

Table 6
Comparison of BVSS for MgO (2×2)-α surface sites.

SII	2×2-α-O1		2×2-α-O2		2×2-α-O3		2×2-α-OH1		2×2-α-OH2		2×2-α-OH3	
	0.46		0.49		0.25		0.22		0.20		0.37	
	Atom	BVS	Atom	BVS	Atom	BVS	Atom	BVS	Atom	BVS	Atom	BVS
Surface	Site 1		O1	-1.83	O1	-1.51	O8	-1.59	H1	0.99	H2	1.00
	Site 2	O1	-2.02		O2	-1.67	H1	1.00	O8	-2.12	O8	-2.23
	Site 3	O2	-0.92	O2	-0.89		O1	-2.28	O1	-1.77	H1	1.00
							H2	1.03	H2	1.03	O1	-2.42
							O2	-1.93	O2	-1.94	O2	-0.90

termination, with a hydrogen bound to each O atom. The ($\sqrt{3}\times\sqrt{3}$)-R30°-MgH structure has a single Mg per ($\sqrt{3}\times\sqrt{3}$) unit cell atop an oxygen termination, with one of the O atoms in the sub-surface layer hydroxylated. The ($\sqrt{3}\times\sqrt{3}$)-OH structure has one O atom and one OH group per ($\sqrt{3}\times\sqrt{3}$) unit cell atop a magnesium termination. The MgH octapole is like the dry Mg octapole, with an OH group in the vacant O position in the second layer, and one other O atom in that layer also hydroxylated. In the OH octapole, the terminal O is hydroxylated, and additional OH group bridges two Mg atoms from the second layer. The (2×2)-α-OH structures are similar to the (2×2)-α-O structures, but all three sites in the α phase are occupied: two by OH groups and one by an O.

The three (2×2)-α-OH structures are similar to the (2×2)-α-O structures (Table 6 and Fig. 7). All three oxygen sites are occupied, and two of three are hydroxylated. The O site stability revealed in the BVS analysis of the (2×2)-α-O structures predicts a stability for the hydroxylated structures of model 2 > model 1 >> model 3. This is exactly what is observed. Model 3, with under-coordinated site 3 not hydroxylated (BVS = -0.90), has the highest DFT calculated energy and the highest SII. In the models where site 3 is hydroxylated, the O atom there is stabilized (BVS = -1.93 or -1.94 for models 1 and 2, respectively). Model 2 is slightly better than model 1 in terms of both SII and DFT energy largely because the non-hydroxylated site in model 2 (BVS = -1.77) is less under-coordinated than the non-hydroxylated site in model 1 (BVS = -1.59).

The bond valence analysis of the dry and hydroxylated (2×2)-α structures agree that if water were to adsorb and dissociate on the surface, the hydroxyl groups would bond most strongly to site 3, and slightly prefer site 1 over site 2. Removal of an H₂O group, conversely, would most likely remove the O from site 3. The bond valence analysis indicates both where water molecules will adsorb and dissociate, and where they are likely to re-associate and desorb. One could even predict from the bond valence sums that heating a MgO (111) (2×2)-α-OH structure to drive off water would cause it to reconstruct to another structure with site 3 unoccupied.

The ($\sqrt{3}\times\sqrt{3}$)-R30° structures are low both in energy, lying only slightly above the convex hull, and in SII (SII = 0.15 and SII = 0.10 for the O and Mg terminations, respectively). In DFT calculations, the O termination is lower in energy, while the Mg termination has BVSS closer to the expected values (Table 7 and Fig. 7). However, the terminal Mg ion has less than half of its coordination sphere occupied, and is unstable according to geometric considerations. The oxygen termination has the terminal O atom only in sites equivalent to site 2 (the most favorable site) of the (2×2) structures, and half are hydroxylated. Ciston and coworkers found ($\sqrt{3}\times\sqrt{3}$)-R30°-OH structure was formed when the (2×2)-α-OH structure was annealed, and concluded that this transition occurred through dehydration and oxygen rearrangement [45]. This is consistent with removal of water from site 3 and the preference for occupancy of site 2 predicted in the (2×2)-α BVS analysis.

The (1×1)-H structure is calculated to be relatively stable,[45] consistent with the bond valence analysis (Table 7 and Fig. 7). The

MgH and OH terminated octapoles are calculated to be low in energy, with the O termination the lower of the two. This agrees well with the bond valence analysis, where they SII is low for both structures but lower for the O termination (SII = 0.09 vs. 0.16, Table 5). Geometric considerations suggest that the MgH octapole is even less stable.

5.2. H₂O on NiO (111)

Ciston and coworkers also examine several structures on the NiO (111) surface, and find that it behaves similarly to the MgO (111) surface [94]. Five dry structures are considered (Ni and O terminated octapoles and three (2×2)-α-O structures), all of which are analogous to an MgO structure described above. Additionally, six of seven hydroxylated structures considered (Ni and O terminated $\sqrt{3}\times\sqrt{3}$ -R30° structures, three (2×2)-α-OH structures, and a (1×1)-H structure) are analogous to MgO structures considered above, with the final structure considered being the (2×2)-vac structure considered first in Erdman et al.[97] This final structure we will set aside for now, as we briefly compare the NiO (111) surface bonding to that of MgO (111).

Before describing the results, one important point needs to be made: NiO is a difficult material for DFT. While relatively high-level methods were used (on-site hybrid exact exchange) they still only have limited accuracy so it should not be a surprise that the BVS in such cases (with DFT calculated positions) is further from the expected value than it is for MgO, despite the strong chemical similarities of the two.

Similar to the MgO (111) surface, among the dry structures, the octapoles have the lowest DFT calculated surface energy and also have the best BVSS (Table 8 and Fig. 8). Also like the MgO surface, the O terminated octapole is lower in energy, while the Ni terminated octapole has a lower SII, but is unstable by geometric considerations. Despite the octapoles having better coordination than any other dry surface, they are still significantly under-coordinated, which results in SII's higher than observed for any stable SrTiO₃ or MgO surface.

The (2×2)-α-O models (Table 9 and Fig. 8) are similar to those for the MgO (111) surface, in that in each model two of the three surface oxygen sites are occupied, with one vacant. As with the MgO surface, the O sites can be ordered in terms of providing sufficient oxygen

Table 7
BVSS for MgO 1×1-H, and $\sqrt{3}\times\sqrt{3}$ -R30° structural models.

SII	1×1-H			$\sqrt{3}\times\sqrt{3}$ -R30°-OH			$\sqrt{3}\times\sqrt{3}$ -R30°-MgH		
	0.18			0.15			0.10		
	Atom	Mult	BVS	Atom	Mult	BVS	Atom	Mult	BVS
Surface	H1	1	1.03	H1	1	1	Mg1	1	1.82
				O1	1	-2.35			
	O4	1	-2.30	O2	1	-1.73			
Sub-Surface	Mg4	1	2.22	Mg1	3	1.99	H1	1	1.03
							O1	1	-2.13
							O3	1	-1.87
							O2	1	-1.92

Table 8
BVSs for NiO (111) octapolar, 1 × 1-H, and √3 × √3-R30° structures.

SII	O-oct			Ni-oct			1 × 1-H			√3 × √3-R30°-OH			√3 × √3-R30°-NiH		
	0.23			0.22			0.13			0.22			0.20		
	Atom	Mult	BVS	Atom	Mult	BVS	Atom	Mult	BVS	Atom	Mult	BVS	Atom	Mult	BVS
Surface	O1	1	-1.57	Ni1	1	1.63	H1	1	1.02	H1	1	1.00	Ni1	1	1.66
							O4	1	-2.20	O1	1	-1.53			
										O2	1	-2.21			
Sub-surface	Ni1	3	1.7	O1	3	-1.75	Ni4	1	2.09	Ni1	3	1.81	H1	1	1.03
													O1	1	-2.12
													O2	1	-1.77
													O3	1	-1.70

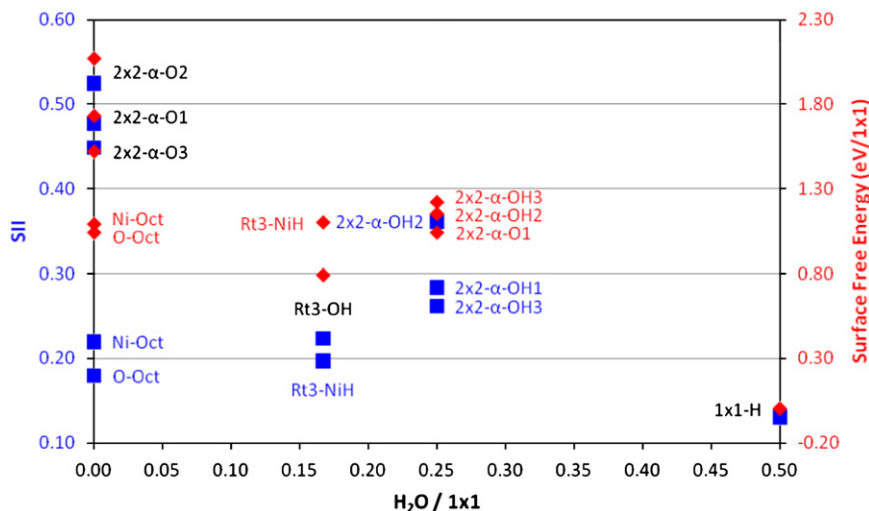


Fig. 8. Comparison of surface free energy [94] and SII for NiO (111) structures.

coordination as: site 2 > site 1 >> site 3. All three models are severely under-coordinated.

For the (2 × 2)-α-OH structures (Table 9 and Fig. 8), as expected, the model with site 2 not hydroxylated (model 3, SII = 0.26) has the best overall coordination, followed by the model with site 1 not hydroxylated (model 1, SII = 0.28), then by the model with site 3 not hydroxylated (model 2, SII = 0.36). The non-hydroxylated O atom is severely under-coordinated in all cases, and is in large part responsible for the high SII in all three models. While these BVSs match with what is expected based on the non-hydroxylated structures and the MgO surface, they are directly opposite the DFT calculated energies [94]. This is the only set of structures for which the BVS and DFT truly disagree, although the DFT energies of the three structures were within error of each other [94].

The (√3 × √3)-R30° structures have lower surface instability indices (0.20 for the nickel termination and 0.22 for the oxygen termination, Table 8 and Fig. 8). Like other structures with a terminal cation, the terminal Ni atom has less than half its coordination sphere filled,

and is thus less stable than indicated by the simple BVS calculation. This qualitatively agrees with the DFT calculations in which the nickel termination is higher in energy than the oxygen termination. For the (√3 × √3)-R30°-OH structure, half of the surface O atoms are hydroxylated and over-coordinated (BVS = -2.21), while the non-hydroxylated half are under-coordinated (BVS = -1.53). As with MgO, Ciston and coworkers found the (√3 × √3)-R30°-OH structure to form through dehydration of the (2 × 2)-α-OH structure [94]. The preference for site 2 and vacancy of site 3 after dehydration is consistent with BVS analysis of the (2 × 2)-α structures.

The (1 × 1)-H structure is also the best coordinated (Table 8 and Fig. 8), with over-coordinated surface O atoms, and slightly over-coordinated Ni atom in the layer immediately below. All the other atoms have coordination near to the bulk values, and the SII is the lowest of all the NiO structures at 0.13.

In general, the instability indices, both surface and global, are high for NiO, due to under-coordination. This is almost certainly due in part to the low BVS for bulk NiO (±1.85) in conjunction with the

Table 9
Comparison of BVSs for NiO (111) (2 × 2)-α surface sites.

SII	2 × 2-α-O1		2 × 2-α-O2		2 × 2-α-O3		2 × 2-α-OH1		2 × 2-α-OH2		2 × 2-α-OH3		
	0.48		0.52		0.45		0.28		0.36		0.26		
	Atom	BVS	Atom	BVS	Atom	BVS	Atom	BVS	Atom	BVS	Atom	BVS	
Surface	Site 1	O1	-1.51	O1	-1.34	O1	-1.36	H1	0.99	H2	0.99	H2	0.99
		O1	-1.68		O2		-1.35		O2		-2.07		O2
	Site 2	O2	-0.96	O2	-0.98	H1	1.02	O3	-0.97	H1	1.02	O3	-1.84
		O2	-1.68		O2		-0.98		O3		-1.82		O3

artifact of the DFT positions as mentioned above. However, the general trends of the BVS do correlate well with the trends of the DFT energies, what is found for MgO and the experimental data. The (2×2) - α -OH results disagree with DFT, but agree with the (2×2) - α -O and MgO (111) results. This implies that BVS analysis may work better than DFT for assessing surface stability, at least for materials which are difficult to deal with via DFT.

6. Conclusions

Chemical bonding goes far in explaining surface structure stability, with a simple BVS calculation capable of illuminating much of this. It is not a perfect method, but neither is DFT nor any other method. As seen for the MgO- (2×2) - α surfaces, a simple BVS analysis has the power to predict where water is likely to adsorb and dissociate on a surface. Structural models that are most likely to exist as-is are those with the best overall BVSS, i.e. the best SII. Structures with BVSS that are too high (over-coordinated) can certainly form, especially if only a small portion of the structure is over-coordinated, as is demonstrated by the SrTiO₃ (100) $c(4 \times 2)$ surface structure. Structures which are somewhat under-coordinated may likewise form, although such structures are likely to adsorb foreign species. A structure without any under-coordinated species on the surface might be more robust and less likely to adsorb any foreign species. Conversely, something on an over-coordinated surface structure might dissociate in order to lower the coordination. Cases where the SII are all rather high are probably not those of lowest energy, as the numbers indicate for the SrTiO₃ (111) surface. Note that from the DFT energies alone one could not reach such a conclusion.

Chemical bonding models of surfaces generally agree with physics based calculations and with experiment, just as they do for bulk structures. In most cases where the SII and DFT calculated energy disagree, other chemical bonding theories which account for geometry help explain this discrepancy. Additionally, the bond valence model has been shown to easily describe concepts, such as polar surfaces, which have been most difficult to deal with from a purely physics based approach. In some cases BVS may help for systems which are difficult for DFT. In the most difficult cases, it may prove necessary to use chemical and physics based methods in conjunction to achieve the most complete understanding of a surface. For instance, the fact that in DFT the $(\sqrt{2} \times \sqrt{2})$ -R45° (001) SrTiO₃ surface has the lowest energy, but it does not have the lowest SII implies that there might be a problem with this surface where DFT (without exact-exchange on the oxygen atoms) is underestimating the oxygen-oxygen non-bonded repulsions.

It is clear that, moving forward, a chemical bonding approach should be considered as a part of any surface study. The complementary nature of the chemistry and physics based models can lead to a greatly enhanced understanding of surface structure, chemistry, and reactivity. As with bulk materials, the best way to move forward is to consider the chemistry and physics simultaneously, with each providing insight that is difficult to reach from the alternate approach.

Acknowledgements

This work was supported primarily by the Institute for Catalysis in Energy Processing, a collaborative research effort between the Northwestern University Center for Catalysis and Surface Science and Argonne National Laboratory, funded through the US Department of Energy, Office of Basic Energy Science (award number DE-FG02-03-ER15457). AEB acknowledges support by the Department of Energy on Grant Number DE-FG02-01ER45945. We also acknowledge funding for a computational cluster for the DFT calculations from the National Science Foundation on Grant Number DMR 0906306 and the Department of Energy on Grant Number DE-FG02-01ER45945. JAE acknowledges support from Argonne National Laboratory. The

submitted manuscript has been created by Argonne National Laboratory, a U.S. Department of Energy Office of Science Laboratory, operated by UChicago Argonne, LLC. The U.S. Government retains for itself, and others acting on its behalf, a paid-up nonexclusive, irrevocable worldwide license in said article to reproduce, prepare derivative works, distribute copies to the public, and perform publicly and display publicly, by or on behalf of the Government.

Appendix A. Supplementary data

Supplementary data to this article can be found online at doi:10.1016/j.susc.2011.10.018.

References

- [1] M.D. Pashley, Phys. Rev. B: Condens. Matter 40 (1989).
- [2] D. Wolf, Phys. Rev. Lett. 68 (1992).
- [3] C. Noguera, J. Phys. Condens. Matter 12 (2000).
- [4] D.S. Deak, Mater. Sci. Technol. 23 (2007).
- [5] J. Goniakowski, F. Finocchi, C. Noguera, Rep. Prog. Phys. 71 (2008) 016501.
- [6] J.A. Enterkin, A.K. Subramanian, B.C. Russell, M.R. Castell, K.R. Poeppelmeier, L.D. Marks, Nat. Mater. 9 (2010).
- [7] I.D. Brown, D. Altermatt, Acta Crystallogr., Sect. B: Struct. Sci. 41 (1985).
- [8] I.D. Brown, The chemical bond in inorganic chemistry: the bond valence model, Oxford; New York, Oxford University Press, 2002.
- [9] I.D. Brown, Chem. Rev. 109 (2009).
- [10] L. Pauling, J. Am. Chem. Soc. 51 (1929) 1010.
- [11] R.F.W. Bader, Chemical Reviews, 91, 1991.
- [12] I.D. Brown, Acta Crystallogr., Sect. B: Struct. Sci. 48 (1992).
- [13] M. Isobe, M. Onoda, T. Ohta, F. Izumi, K. Kimoto, E. Takayama-Muromachi, A.W. Hewat, K. Ohoyama, Phys. Rev. B: Condens. Matter 62 (2000).
- [14] R. Tamazyan, S. van Smaalen, I.G. Vasilyeva, H. Arnold, Acta Crystallogr., Sect. B: Struct. Sci. 59 (2003).
- [15] S. van Smaalen, R. Dinnebier, M. Sofin, M. Jansen, Acta Crystallogr., Sect. B: Struct. Sci. 63 (2007).
- [16] D.F. Xue, S. Zuo, H. Ratajczak, Physica B 352 (2004).
- [17] R.Q. Albuquerque, G.B. Rocha, O.L. Malta, P. Porcher, Chem. Phys. Lett. 331 (2000).
- [18] D.F. Xue, S.Y. Zhang, Physica B 262 (1999).
- [19] D. Xue, K. Betzler, H. Hesse, Appl. Phys. A Mater. Sci. Process. 74 (2002).
- [20] V.M. Holovey, V.I. Sidey, V.I. Lyamayev, M.M. Bairov, J. Phys. Chem. Solids 68 (2007).
- [21] V.M. Holovey, V.I. Sidey, V.I. Lyamayev, P.P. Puga, J. Lumin. 126 (2007).
- [22] Y. Tabira, R.L. Withers, Phys. Chem. Miner. 27 (1999).
- [23] S. Adams, J. Swenson, Ionics 10 (2004).
- [24] M. Newville, Phys. Scr. T115 (2005).
- [25] T. Hiemstra, W.H. Vanriemsdijk, G.H. Bolt, J. Colloid Interface Sci. 133 (1989).
- [26] T. Hiemstra, P. Venema, W.H. Vanriemsdijk, J. Colloid Interface Sci. 184 (1996).
- [27] B.R. Bickmore, K.M. Rosso, K.L. Nagy, R.T. Cygan, C.J. Tadanier, Clays Clay Miner. 51 (2003).
- [28] B.R. Bickmore, C.J. Tadanier, K.M. Rosso, W.D. Monn, D.L. Eggett, Geochim. Cosmochim. Acta 68 (2004).
- [29] M. Schindler, A. Mutter, F.C. Hawthorne, A. Putnis, Can. Mineral. 42 (2004).
- [30] B.R. Bickmore, K.M. Rosso, C.J. Tadanier, E.J. Bylaska, D. Doud, Geochim. Cosmochim. Acta 70 (2006).
- [31] C. Ruberto, Y. Yourdshahyan, B.I. Lundqvist, Phys. Rev. Lett. 88 (2002) 226101.
- [32] C. Ruberto, Y. Yourdshahyan, B.I. Lundqvist, Phys. Rev. B: Condens. Matter 67 (2003) 195412.
- [33] L.D. Marks, A.N. Chiamonti, F. Tran, P. Blaha, Surf. Sci. 603 (2009).
- [34] N. Erdman, K.R. Poeppelmeier, M. Asta, O. Warschkow, D.E. Ellis, L.D. Marks, Nature 419 (2002).
- [35] N. Erdman, O. Warschkow, M. Asta, K.R. Poeppelmeier, D.E. Ellis, L.D. Marks, J. Am. Chem. Soc. 125 (2003) 10050.
- [36] O. Warschkow, M. Asta, N. Erdman, K.R. Poeppelmeier, D.E. Ellis, L.D. Marks, Surf. Sci. 573 (2004) 446.
- [37] G.J. Palenik, Inorg. Chem. 36 (1997).
- [38] K. Knížek, Kalvados, 2010.
- [39] A.E.H. Love, A Treatise on the Mathematical Theory of Elasticity, Dover Publications, 1892.
- [40] L.D. Marks, P. Xu, D.N. Dunn, Surf. Sci. 294 (1993).
- [41] S.J. Thompson, S.P. Lewis, Phys. Rev. B: Condens. Matter 73 (2006).
- [42] P. Blaha, K. Schwarz, G.K.H. Madsen, D. Kvasnicka, J. Luitz, WIEN2k, An Augmented Plane Wave Plus Local Orbitals Program for Calculating Crystal Properties, Technical University of Vienna, Vienna, 2001.
- [43] J.P. Perdew, K. Burke, M. Ernzerhof, Phys. Rev. Lett. 77 (1996) 3865.
- [44] I. Etxebarria, J.M. Perez-Mato, A. Garcia, P. Blaha, K. Schwarz, J. Rodriguez-Carvajal, Phys. Rev. B: Condens. Matter 72 (2005) 174108.
- [45] J. Ciston, A. Subramanian, L.D. Marks, Phys. Rev. B: Condens. Matter 79 (2009) 085421.
- [46] P. Muller, A. Saul, Surf. Sci. Rep. 54 (2004).
- [47] J.P. Perdew, A. Ruzsinszky, G.I. Csonka, O.A. Vydrov, G.E. Scuseria, L.A. Constantin, X.L. Zhou, K. Burke, Phys. Rev. Lett. 100 (2008) 136406.
- [48] A. Stroppa, G. Kresse, New J. Phys. 10 (2008).

- [49] J.P. Perdew, A. Ruzsinszky, G.I. Csonka, L.A. Constantin, J.W. Sun, *Phys. Rev. Lett.* 103 (2009).
- [50] E. Heifets, E.A. Kotomin, G. Borstel, *Surf. Rev. Lett.* 6 (1999).
- [51] E. Heifets, E.A. Kotomin, *Thin Solid Films* 358 (2000).
- [52] E. Heifets, E.A. Kotomin, J. Maier, *Surf. Sci.* 462 (2000).
- [53] F. Bottin, F. Finocchi, C. Noguera, *Phys. Rev. B: Condens. Matter* 68 (2003).
- [54] F. Bottin, F. Finocchi, C. Noguera, *Surf. Sci.* 532 (2003) 468.
- [55] E. Heifets, W.A. Goddard, E.A. Kotomin, R.I. Eglitis, G. Borstel, *Phys. Rev. B: Condens. Matter* 69 (2004).
- [56] E.A. Kotomin, E. Heifets, S. Dorfman, D. Fuks, A. Gordon, J. Maier, *Surf. Sci.* 566 (2004).
- [57] F. Bottin, F. Finocchi, C. Noguera, *Surf. Sci.* 574 (2005).
- [58] R.I. Eglitis, D. Vanderbilt, *Phys. Rev. B: Condens. Matter* 77 (2008) 195408.
- [59] M. Lazzeri, A. Selloni, *Phys. Rev. Lett.* 87 (2001).
- [60] R.J. Gillespie, R.S. Nyholm, *Q. Rev. Chem. Soc.* 11 (1957) 339.
- [61] M.A. Harvey, S. Baggio, R. Baggio, *Acta Crystallogr., Sect. B: Struct. Sci.* 62 (2006).
- [62] L.D. Marks, A.N. Chiamonti, F. Tran, P. Blaha, CIF depository for "The small unit cell reconstructions of SrTiO₃ (111)", 2009.
- [63] A.N. Chiamonti, C.H. Lanier, L.D. Marks, P.C. Stair, *Surf. Sci.* 602 (2008).
- [64] M. Naito, H. Sato, *Physica C* 229 (1994).
- [65] M.R. Castell, *Surf. Sci.* 505 (2002).
- [66] N. Erdman, L.D. Marks, *Surf. Sci.* 526 (2003).
- [67] K. Johnston, M.R. Castell, A.T. Paxton, M.W. Finnis, *Phys. Rev. B: Condens. Matter* 70 (2004) 085415.
- [68] N. Iles, F. Finocchi, K.D. Khodja, *J. Phys. Condens. Matter* 22 (2010).
- [69] Q.D. Jiang, J. Zegenhagen, *Surf. Sci.* 338 (1995).
- [70] R. Herger, P.R. Willmott, O. Bunk, C.M. Schlepütz, B.D. Patterson, B. Delley, *Phys. Rev. Lett.* 98 (2007) 076102.
- [71] R. Herger, P.R. Willmott, O. Bunk, C.M. Schlepütz, B.D. Patterson, B. Delley, V.L. Shneerson, P.F. Lyman, D.K. Saldin, *Phys. Rev. B: Condens. Matter* 76 (2007) 195435.
- [72] Q.D. Jiang, J. Zegenhagen, *Surf. Sci.* 425 (1999).
- [73] M.R. Castell, *Surf. Sci.* 516 (2002).
- [74] E. Heifets, S. Dorfman, D. Fuks, E. Kotomin, A. Gordon, *J. Phys. Condens. Matter* 10 (1998).
- [75] Z.Q. Li, J.L. Zhu, C.Q. Wu, Z. Tang, Y. Kawazoe, *Phys. Rev. B: Condens. Matter* 58 (1998).
- [76] G. Charlton, S. Brennan, C.A. Muryn, R. McGrath, D. Norman, T.S. Turner, G. Thornton, *Surf. Sci.* 457 (2000).
- [77] C. Cheng, K. Kunc, M.H. Lee, *Phys. Rev. B: Condens. Matter* 62 (2000).
- [78] E. Heifets, R.I. Eglitis, E.A. Kotomin, J. Maier, G. Borstel, *Phys. Rev. B: Condens. Matter* 64 (2001) 235417.
- [79] T. Kubo, H. Nozoye, *Phys. Rev. Lett.* 86 (2001).
- [80] T. Kubo, H. Nozoye, *Surf. Sci.* 542 (2003).
- [81] L.M. Liborio, C.G. Sanchez, A.T. Paxton, M.W. Finnis, *J. Phys. Condens. Matter* 17 (2005).
- [82] H. Tanaka, T. Matsumoto, T. Kawai, S. Kawai, *Jpn. J. Appl. Phys., Part 1* 32 (1993).
- [83] T. Matsumoto, H. Tanaka, K. Kouguchi, T. Kawai, S. Kawai, *Surf. Sci.* 312 (1994).
- [84] S. Kimura, M. Tsukada, *Appl. Surf. Sci.* 121 (1997).
- [85] D.K. Seo, K. Perdue, J. Ren, M.H. Whangbo, *Surf. Sci.* 370 (1997).
- [86] A. Stashans, F. Erazo, J. Ortiz, P. Valverde, *Philos. Mag. B* 81 (2001).
- [87] C.H. Lanier, A. van de Walle, N. Erdman, E. Landree, O. Warschkow, A. Kazimirov, K.R. Poeppelmeier, J. Zegenhagen, M. Asta, L.D. Marks, *Phys. Rev. B: Condens. Matter* 76 (2007) 045421.
- [88] S. Tinte, M.G. Stachiotti, C.O. Rodriguez, D.L. Novikov, N.E. Christensen, *Phys. Rev. B: Condens. Matter* 58 (1998).
- [89] Z.G. Wu, R.E. Cohen, D.J. Singh, *Phys. Rev. B: Condens. Matter* 70 (2004).
- [90] E. Heifets, E. Kotomin, V.A. Trepakov, *J. Phys. Condens. Matter* 18 (2006).
- [91] R. Armiento, A.E. Mattsson, *Phys. Rev. B: Condens. Matter* 72 (2005) 085108.
- [92] L. Schimka, J. Harl, G. Kresse, *J. Chem. Phys.* 134 (2011) 024116.
- [93] A.E. Becerra-Toledo, J.A. Enterkin, D. Kienzle, L.D. Marks, Water adsorption on SrTiO₃(001): II. water, water, everywhere, *Surf. Sci.* (submitted for publication). Manuscript Number: SUSC-D-11-00528R1.
- [94] J. Ciston, A. Subramanian, D. Kienzle, L.D. Marks, *Surf. Sci.* 604 (2010) 155.
- [95] F. Finocchi, A. Barbier, J. Jupille, C. Noguera, *Phys. Rev. Lett.* 92 (2004).
- [96] W.B. Zhang, B.Y. Tang, *J. Phys. Chem. C* 112 (2008).
- [97] N. Erdman, O. Warschkow, D.E. Ellis, L.D. Marks, *Surf. Sci.* 470 (2000).